photonics

MDPI

Article

Dynamic Behaviors of Pulsating Noise-like Pulses in an Ultrafast Fiber Laser

Lei Zhang [1,2], Pinghua Tang [3], Jinhai Zhu [1], Zexin Zhou [1], Haitao Wu [1] and Zhenhong Wang [1,*]

[1] College of Electronics and Information Engineering, Shenzhen University, Shenzhen 518060, China; 2210434005@email.szu.edu.cn (L.Z.); 2310434049@email.szu.edu.cn (J.Z.); 2310434034@email.szu.edu.cn (Z.Z.); 2410044046@mails.szu.edu.cn (H.W.)
[2] Zhejiang HiThink RoyalFlush AI Research Institute, Hangzhou 310012, China
[3] School of Physics and Optoelectronics, Xiangtan University, Xiangtan 411105, China; pinghuatang@xtu.edu.cn
* Correspondence: wangzhenhong@szu.edu.cn

Abstract

In this study, we demonstrate the generation and observation of noise-like pulses (NLPs) with unique pulsating characteristics in an ultrafast fiber laser. Furthermore, these NLPs display distinct periodic intensity modulation during temporal evolution, and the corresponding shot-to-shot spectra based on the dispersive Fourier transform (DFT) method exhibit chaotic characteristics with random variable envelopes in each period. Notably, the pulsating period of these NLPs decreases with the increment of pump power. Moreover, both the average output power and pulse energy show a clear linear growth trend as the pump power is raised. Numerical simulations are further conducted to validate these experimental findings. This work will enrich the study of NLPs and pulsation dynamics and provide valuable insights for the development of ultrafast fiber lasers.

Keywords: fiber lasers; mode locking; noise-like pulses; pulsating pulses; real-time dynamics

1. Introduction

Passively mode-locked fiber lasers (PMLFLs) have emerged as a pivotal platform for generating ultrashort optical pulses with exceptional stability, compact structure, and robust operation [1]. Furthermore, PMLFLs have become indispensable for underpinning critical applications, such as industrial micromachining, medical surgery, and optical communications [2–4]. Equally important, these lasers can serve as versatile testbeds for exploring nonlinear phenomena and soliton dynamics [5,6], further reinforcing their central position in ultrafast photonics. Typically, under the interplay of nonlinearity, dispersion, loss, and gain, fiber lasers can achieve various stable mode-locking regimes that emit ultrashort pulses with a fixed repetition rate, such as conventional solitons (CS) [7], dissipative solitons [8], and harmonic pulses [9]. However, under specific parameter conditions, the steady state of the system is disrupted, leading to various unstable pulse outputs [10], soliton rains [11], noise-like pulses (NLPs) [12], rogue waves [8,13], soliton explosions [14,15], and pulsating solitons [16]. In the pulsating regime, the pulse energy and peak power of solitons oscillate periodically, presenting a complex and intricating landscape of transient dynamics [17,18]. Furthermore, theoretical studies predict that the pulse energy of pulsating solitons can vary by more than two orders of magnitude within a single pulsation cycle, thereby providing a potential pathway to high-peak-power pulse generation in ultrafast laser systems [19].

check for updates

Received: 26 August 2025
Revised: 15 September 2025
Accepted: 16 September 2025
Published: 19 September 2025

Citation: Zhang, L.; Tang, P.; Zhu, J.; Zhou, Z.; Wu, H.; Wang, Z. Dynamic Behaviors of Pulsating Noise-like Pulses in an Ultrafast Fiber Laser. *Photonics* **2025**, *12*, 937. https://doi.org/10.3390/photonics12090937

Soliton pulsation is a classic example of non-stationary oscillatory pulse structures in ultrafast fiber lasers. In recent years, leveraging the dispersive Fourier Transform (DFT) technology, researchers have gained extensive insight into the transient dynamics of these solitons [20–22]. Pulsating solitons generally correspond to periodic attractors in dissipative systems, acting as the transitional state between stationary solitons and chaotic pulses [20]. By exploring the complex Ginzburg–Landau equation (CGLE), a variety of pulsating phenomena have been theoretically predicted or investigated [23–25]. He et al. investigated the influence of gain dynamics on pulsating solitons is numerically based on generalized CGLE [19]. Afterwards, Wang et al. demonstrated the soliton pulsating dynamics in an L-band PMLFL via the DFT technique, finding that these pulsations have typical features, such as energy oscillation, bandwidth breathing, and temporal shift [21]. Although pulsating solitons have already been reported in experimental and numerical studies, noise-like pulses (NLPs) with pulsating characteristics remain largely understudied. Notably, the synergy between the broadband high-energy bursts of NLPs and the periodic energy oscillation of soliton pulsation will offer a promising route to surpassing the energy ceiling of conventional ultrashort pulses.

In this work, we experimentally report the generation and observation of pulsating NLPs in an ultrafast fiber laser based on a nonlinear polarization rotation (NPR) structure. By properly tuning the intracavity polarization state and pump power, the stable soliton pulses and NLPs with pulsating characteristics are achieved at proper condition. By utilizing DFT-based real-time analysis of transient dynamics, it can be found that the pulsating NLPs exhibit significant periodic variations in spectral energy. Within each period, the pulse envelope comprises numerous sub-pulses with random intensities and envelopes, revealing its intrinsic chaotic properties. When the pump power is adjusted, the corresponding pulsating period varies significantly. Additionally, numerical simulations are conducted to verify the experimental findings. These results substantially enrich the research on NLP dynamics and hold significant value for advancing ultrafast fiber lasers and the broader field of pulsating NLP dynamics.

2. Experimental Setup

The schematic diagram of the PMLFL is shown in Figure 1. To provide sufficient gain, a 1-m-long erbium-doped fiber (nLIGHT Liekki Er80-8/125, EDF, Vancouver, WA, USA) serves as the gain medium, pumped by a 980 nm laser diode. This EDF exhibits a small-signal gain of approximately 0.84 [26], and its third-order dispersion coefficient is about 0.12 ps^3/km at 1560 nm [27]. The pump light is coupled into the cavity via a wavelength-division multiplexer (WDM). Mode locking is achieved through the NPR structure, which comprises two polarization controllers (PCs) and an in-line polarizer (ILP). Additionally, a polarization-independent isolator (PI-ISO) is inserted into the cavity to ensure unidirectional laser propagation. A 30% port of an optical coupler (OC) is used for laser output. It is worth noting that all pigtails of these components are standard single-mode fibers (SMFs). The total cavity length is about 11.88 m, and the net cavity dispersion is about $-0.27\ ps^2$, estimated based on the dispersion coefficients of the EDF and SMF at 1550 nm ($-20\ ps^2/km$ and $-23\ ps^2/km$, respectively). The output characteristics are monitored using an optical spectrum analyzer (Yokogawa, AQ6370D, Tokyo, Japan), a 4 GHz high-speed oscilloscope (Rohde and Schwarz, RTP044, Munich, Germany)), a radio-frequency (RF) spectrum analyzer (Siglent, SSA5023A, Shenzhen, China), and a commercial autocorrelator (APE-150, Pulsecheck, Berlin, Germany).

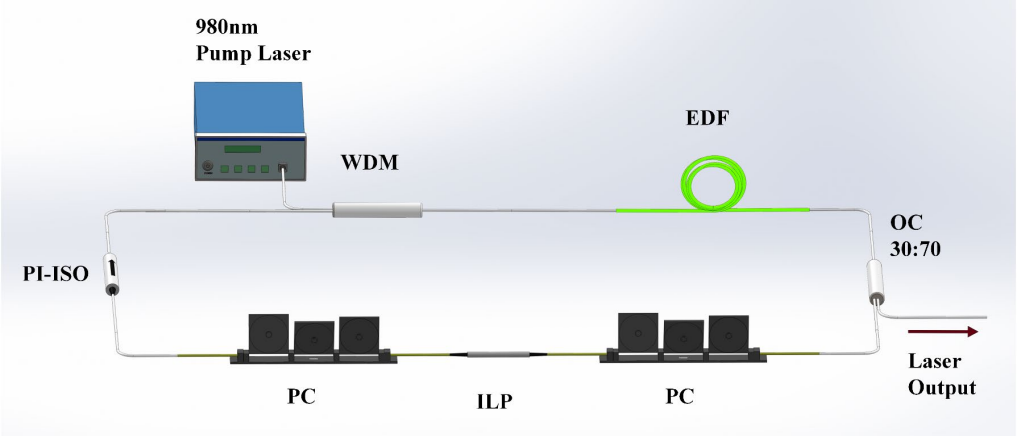

Figure 1. Schematic of the mode-locking fiber laser.

3. Results and Discussion

When the pump power is set to 41 mW and the PCs are finely adjusted to an appropriate state, the stable mode-locked operation can be obtained, as illustrated in Figure 2. Figure 2a presents the measured optical spectrum with a central wavelength of approximately 1566.26 nm and a 3-dB bandwidth of about 6.8 nm. The clear Kelly sidebands appear on both sides of the spectra, indicating that the laser operates under anomalous dispersion. The temporal pulse trains are shown in Figure 2b, exhibiting a pulse-to-pulse interval of ~59.4 ns, which is consistent with the cavity length. To ensure the clarity and stability of the RF signals, the scan width and the resolution bandwidth of the RF spectrum analyzer are set to 1 MHz and 100 Hz, respectively. The corresponding result is depicted in Figure 2c, showing a sharp peak at the repetition frequency of 16.83 MHz with a signal-to-noise ratio (SNR) exceeding 48 dB. This not only matches the cavity round-trip frequency but also confirms low-noise operation. Furthermore, a segment of the dispersion-compensating fiber (DCF) is employed as the dispersive element for DFT measurement, providing a spectral resolution of approximately 0.774 nm. The corresponding DFT monitoring results are presented in Figure 2d, which plots a two-dimensional (2D) successive spectrum over nearly 3500 cavity roundtrips (RTs). A bright and broad stripe is visible at the central wavelength of 1566 nm, surrounded by three weaker narrow bands that are marked with white dashed lines. Their intensities decrease sequentially from “a” to “c”, corresponding precisely to the three spectral peaks (“a”, “b”, and “c”) observed on the spectrum, as shown in Figure 2a. The distinct correspondence in both intensity and position confirms that the DFT process effectively resolves the real-time spectral features. In addition, the output power of the laser is measured to be approximately 2.1 mW, corresponding to the average pulse energy of about 0.12 nJ.

NLPs, as a common phenomenon in the passively mode-locked fiber lasers, can be generated under high-gain conditions, and their characteristics and formation mechanisms have been extensively investigated [12,28]. Benefiting from sufficient gain of the used gain fiber, by gradually increasing the pump power to 413 mW and appropriately changing the paddles of PCs, the NLPs regime is achieved, as depicted in Figure 3. Figure 3a displays the optical spectrum. In contrast to the result in Figure 2a, the spectrum undergoes rapid broadening with the sidebands being suppressed, yielding a smooth spectral profile. The central wavelength is approximately 1562.54 nm with a 3 dB bandwidth of 11.76 nm. The slight shift in the central wavelength is primarily attributed to the inherent filtering effect in the NPR mechanism [29]. Notably, Figure 3b displays pulse trains of approximately 80 μs, accompanied by intense periodic oscillations, suggesting that the NLPs possess pulsating properties. The inset confirms that the interval between adjacent pulses is about 59.4 ns. The RF spectrum reveals a symmetric noise pedestal on both sides of the fundamental

frequency (~16.83 MHz) peak, as illustrated in Figure 3c. The SNR of the central peak is about 54 dB, indicating that the operation maintains relative stability. In addition, the autocorrelation trace, shown in Figure 3d, features a sharp peak of ~7.36 ps in width sitting on a broad pedestal of ~117.7 ps. These observations are basically consistent with the typical characteristics of NLPs [30,31].

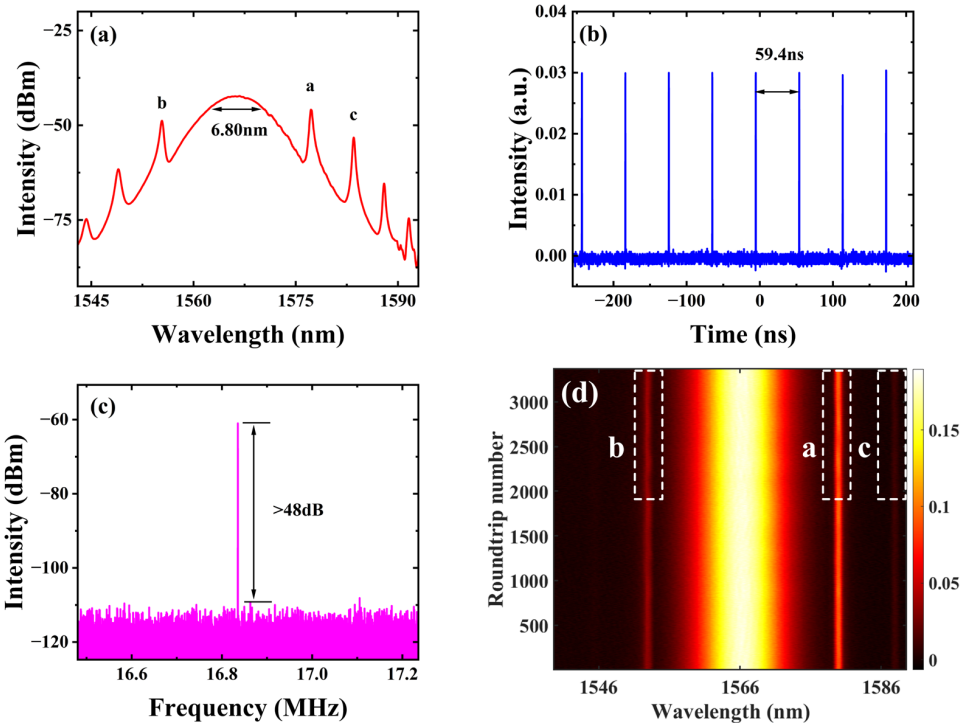

Figure 2. Characteristics of mode-locking state at 41 mW. (**a**) Optical spectrum. (**b**) Pulse trains. (**c**) RF spectrum. (**d**) Two-dimensional shot-to-shot spectra.

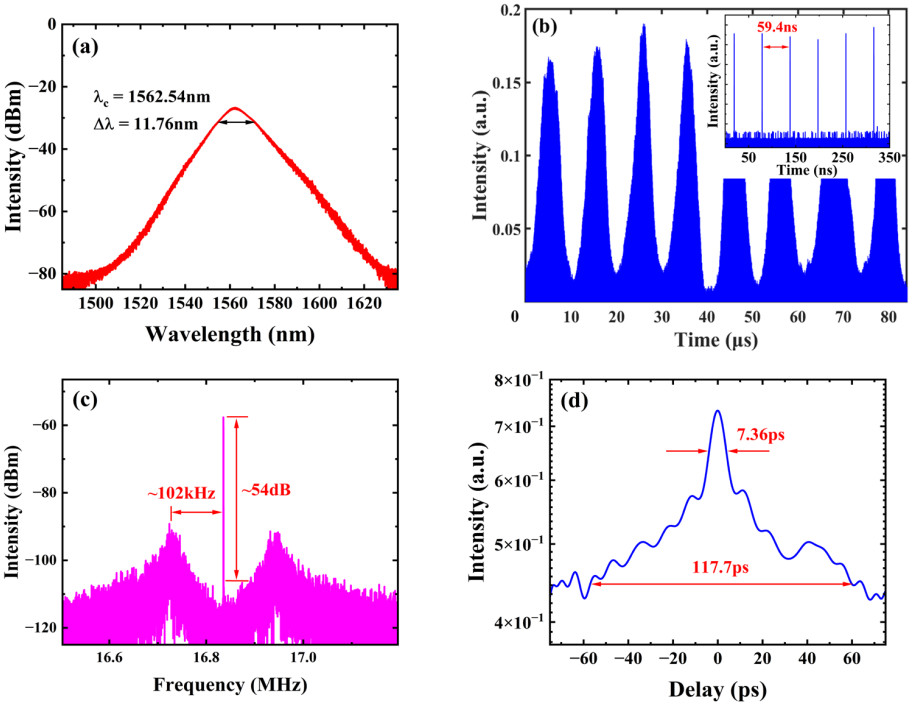

Figure 3. Characteristics of special NLPs at 413 mW. (**a**) Optical spectrum. (**b**) Pulse trains over 80 μs (inset: the details of the pulse trains in the small-time window). (**c**) RF spectrum. (**d**) The autocorrelation trace.

To investigate deeper into the pulsation characteristics of NLPs, the corresponding shot-to-shot spectra are measured by using the DFT technique. Figure 4 reveals the temporal and spectral evolution of the pulsating NLPs at a pump power of 413 mW. Figure 4a presents the temporal evolution of the pulse over 1000 cavity roundtrips. It is evident that the pulse intensity undergoes a transition from a maximum to a minimum after a certain number of roundtrips and then recovers after the same numbers. The period of fluctuation is about 165 roundtrips, corresponding to a time length of 9.801 μs. According to the principle of Fourier transform, this time length basically matches the frequency spacing (~102 kHz) between the central peak and the pedestal observed in Figure 3c. This characteristic further confirms the pulsating properties of the output pulses [16,32]. Figure 4b shows the shot-to-shot spectral evolution over the consecutive cavity roundtrips, exhibiting obvious breathing behaviors with periodic oscillation. Notably, the spectral evolution follows a periodic envelope with random intensity fluctuations in the spectrum, suggesting that these pulses are composed of numerous sub-pulses with randomly varying intensities, that is also a signature of their chaotic property. Additionally, the intracavity pulse energy is evaluated, as shown in the inset. The energy curve in white exhibits localized fluctuations with distinct variations in the maximum and minimum values across successive roundtrips. This behavior can be ascribed to the formation of pulse packets composed of randomly varying sub-pulses. Actually, the wavelength-dependent gain saturation plays a significant role in the periodic oscillation of energy [33].

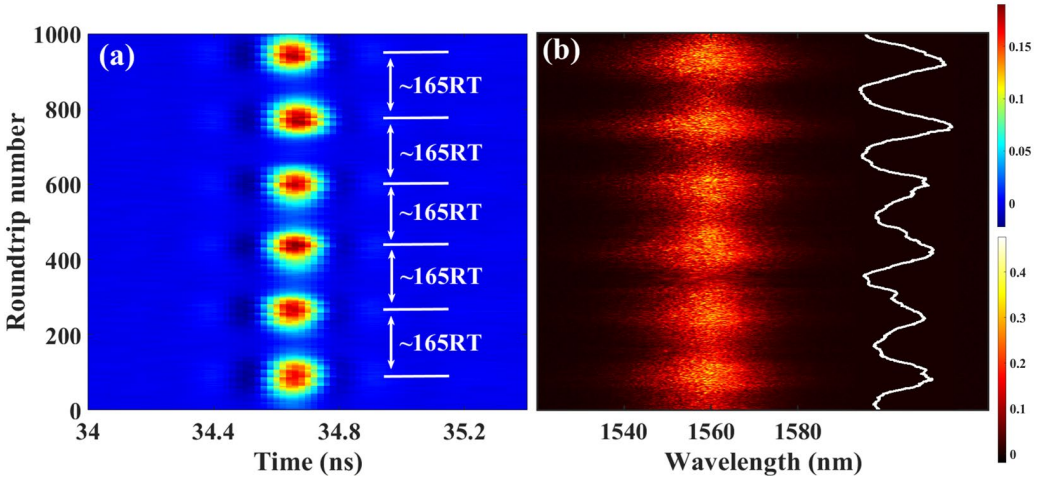

Figure 4. Characteristics of pulsating NLPs at 413 mW. (**a**) Two-dimensional pulse evolutions and (**b**) two-dimensional spectral evolutions (inset: the evolution of the average energy within the cavity) over 1000 roundtrips (RTs).

With the intracavity angles of PCs fixed, the dependence of the pulsation characteristics of NLPs with pump power is investigated, as illustrated in Figure 5. Figures 5a and 5b present the detailed 3D spectral evolution at pump powers of 613 mW and 913 mW, respectively. The pulsation period is approximately 127 cavity roundtrips at 613 mW, corresponding to a temporal interval of ~7.54 μs. The corresponding RF spectrum, shown in Figure 5c, shows a frequency spacing of ~132 kHz, which agrees with the pulsation period. When the pump power is increased to 913 mW, the pulsation period decreases to about 107 roundtrips, equivalent to ~6.36 μs. This observation is consistent with the frequency spacing of the RF spectrum presented in Figure 5d. In addition, the SNRs of the peaks in Figure 5c,d both exceed 60 dB, indicating the good stability of the pulsating NLPs. Figure 5e,f clearly demonstrates that with increasing pump power, both the intensity and the pedestal width of the autocorrelation traces increase significantly. This indicates that the average output power and the temporal duration of the NLP packets become larger.

Furthermore, the relationships among pulsation period, average output power, and pulse energy with pump power are depicted in Figure 6. Figure 6a reveals that the pulsation period decreases continuously with increasing pump power, while Figure 6b shows that both the average output power and pulse energy increase nearly linearly with pump power. Notably, due to the intrinsic nature of NLPs, the pulse energy corresponds to the average energy of the pulse packet formed by lots of sub-pulses, calculated from the average output power and the repetition rate. The maximum average output power achieved is approximately 59.9 mW, corresponding to an average pulse energy of about 3.56 nJ. To verify the stability of the pulse output, continuous two-hour periodic measurements of the average output power were conducted, with the results shown in Figure 7. The overall power level exhibits a favorable trend, demonstrating the relative stability of the laser system.

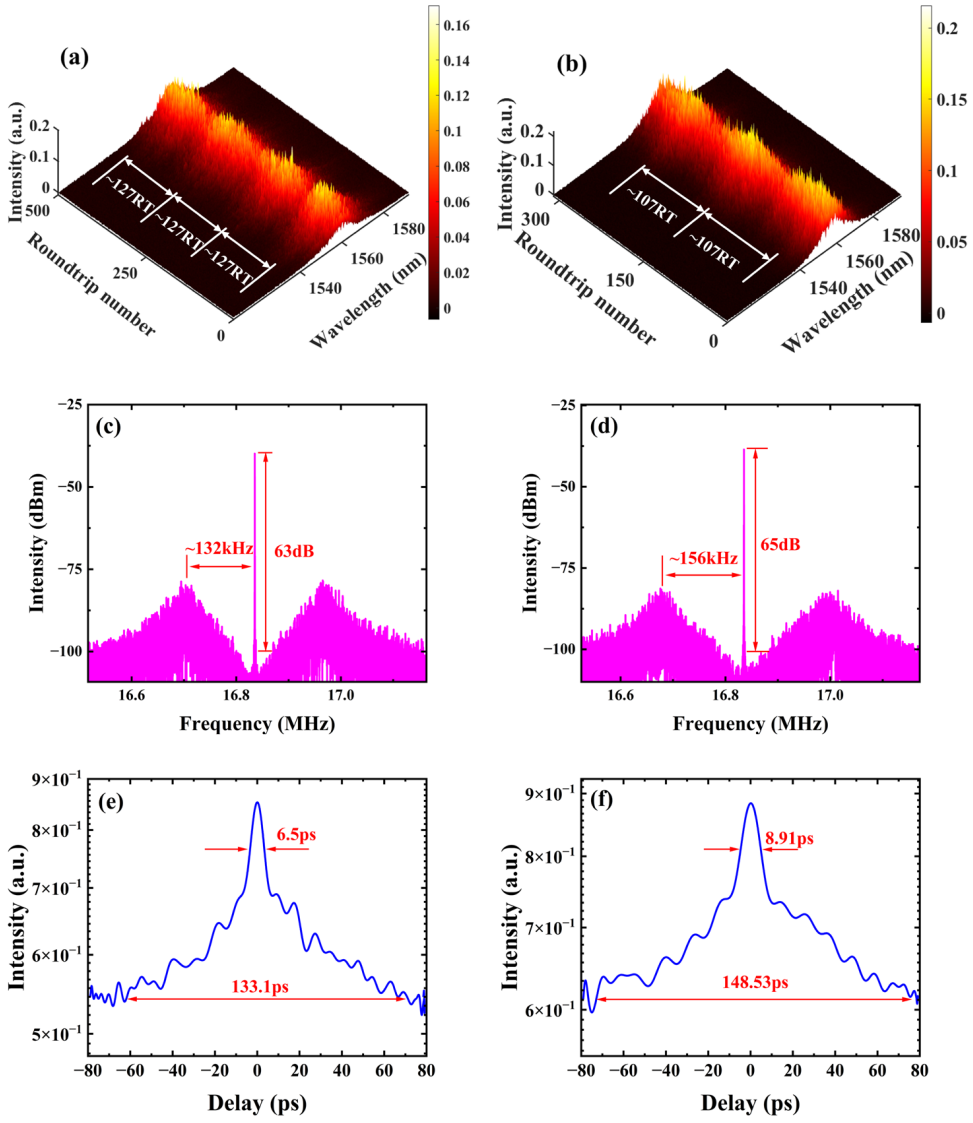

Figure 5. Three-dimensional spectral evolution over 300 roundtrips (RTs) at (**a**) 613 mW and (**b**) 913 mW, (**c**,**d**) corresponding to the measured RF spectrum and (**e**,**f**) the autocorrelation trace.

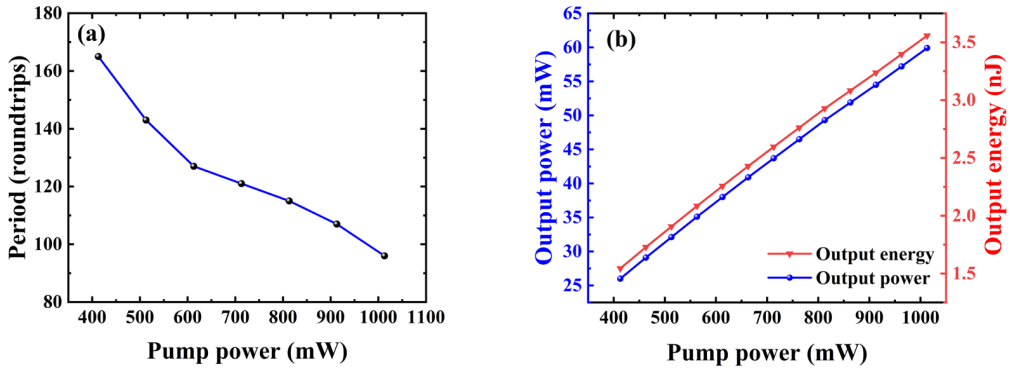

Figure 6. (**a**) The period of pulsating NLPs and (**b**) average output power and output energy with different pump powers.

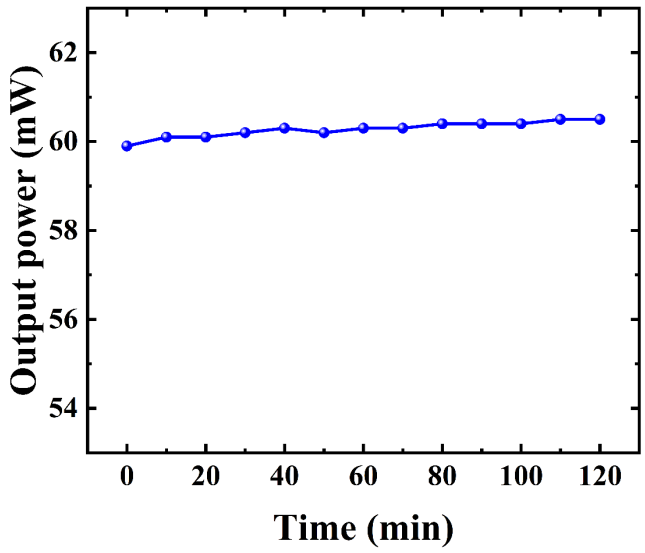

Figure 7. The output power over time at a pump power of 1013 mW.

4. Numerical Simulation

Numerical simulations of the laser operation are conducted to further qualitatively reconstruct the NLPs with pulsating characteristics. The numerical model is established using the generalized nonlinear Schrödinger equation (GNLSE) [25]:

$$\frac{\partial A}{\partial z} = -\frac{i\beta_2}{2}\frac{\partial^2 A}{\partial t^2} + \frac{g-\alpha}{2}A + \frac{g}{2\Omega^2}\frac{\partial^2 A}{\partial t^2} + i\gamma|A|^2 A \quad (1)$$

Here, A represents the slowly varying amplitude of the pulse envelope, while β_2 denotes the second-order dispersion terms. The variable t corresponds to time in a reference frame that is retarded to follow the pulse's group velocity. γ is the nonlinear coefficient, α accounts for cavity losses, and Ω signifies the 3-dB bandwidth of the gain medium. The saturable gain of the fiber, represented by g, is given by:

$$g = g_0 \exp\left(-\frac{\int |A|^2 dt}{E_{sat}}\right) \quad (2)$$

In this context, g_0 represents the small-signal gain, and E_{sat} denotes the saturation energy of the EDF. When pulses propagate through the passive fiber section, g_0 is set to

zero. Mode-locking in the cavity is achieved through the use of a saturable absorber (SA) with the following power-dependent transfer function:

$$T = 1 - \frac{\alpha_0}{1 + \frac{|A(t)|^2}{I_{sat}}} \tag{3}$$

Here, T denotes the transmittance of the saturable absorber (SA), α_0 represents the modulation depth of the SA, and I_{sat} is the saturation power of the SA.

The numerical model is implemented using a standard symmetric split-step Fourier method. Contributions from dispersion and gain are computed in the frequency domain, while the nonlinear term is evaluated in the time domain. For these simulations, the initial field comprises Gaussian random noise modulated by a sech envelope in the time domain. The parameters used in these simulations are consistent with experimental values. In order to approximate the experiments, we have chosen the following parameters: I_{sat} = 200 W, α_0 = 0.2, α = 0.2 dB/km, Ω = 50 nm. For the lengths of SMF and EDF, we chose to be consistent with the experiments: L_{EDF} = 1 m, $\beta_2 = -20$ ps^2/km, and γ = 1.6 W^{-1} km^{-1}; L_{SMF} = 10.88 m, $\beta_2 = -23$ ps^2/km, and γ = 1.3 W^{-1} km^{-1}. For the OC, the output is 30%.

When the g_0 and E_{sat} values are set to 1 m^{-1} and 1 nJ, respectively, the stable single soliton output can be easily observed, as illustrated in Figure 8. The simulated spectrum is shown in Figure 8a, which is very similar to the fundamental frequency spectrum obtained in our experiment. Moreover, the pulse evolution with more than 200 roundtrips is evaluated, as illustrated in Figure 8b. We can clearly see that after 200 roundtrips, it remains quite stable. Figure 8c shows the pulse profile. We can see that this is a pure single pulse with a width in the ps range, similar to what we obtained in our experiment. Finally, we plotted the energy evolutions as shown in Figure 8d. It remained horizontal throughout more than 200 cycles, demonstrating its stability.

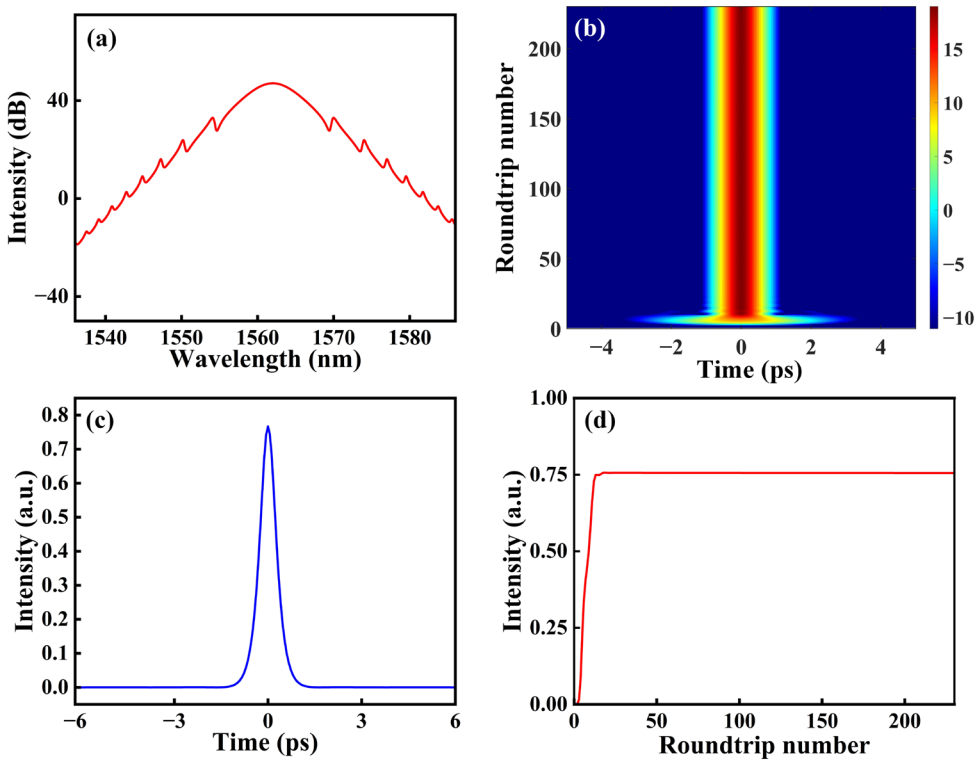

Figure 8. Simulating single-soliton outputs. (**a**) Optical spectrum. (**b**) Pulse evolution. (**c**) Pulse profiles. (**d**) Energy evolutions.

In the experiment, pulsating NLPs start to appear by increasing the pump power. In the simulation, changing the small-signal gain g_0 is equivalent to changing the pump power in the experiment [34]. Thus, the NLP state can be obtained at g_0 = 5 m^{-1}, as depicted in Figure 9. Figure 9a shows the spectral evolution over 200 cycles. Clearly, there are substantial fluctuations on these roundtrip-to-roundtrip spectra, which is a typical spectral characteristic of the NLPs. To investigate the dynamic characteristics, the corresponding energy evolutions are evaluated, as displayed in Figure 9b. The energy curve exhibits a wave-like pattern with periodic variations, suggesting that this pulse operation has pulsating behaviors. Figure 9c displays the corresponding pulse evolutions. Clearly, it can be observed that the initial pulse splits into multiple sub-picosecond pulses with randomly varying intensities and pulse widths through consecutive roundtrips, undergoing a quasi-stable process accompanied by pulse collapse and destruction. In addition, we have studied the effect of g_0, corresponding to the pump power in the experiment, on the pulsation period, as illustrated in Figure 9d. It can be seen that the pulsation period decreases as g_0 increases, and the rate of decrease also slows down. These theoretical results agree well with the experimental results in Figure 6a.

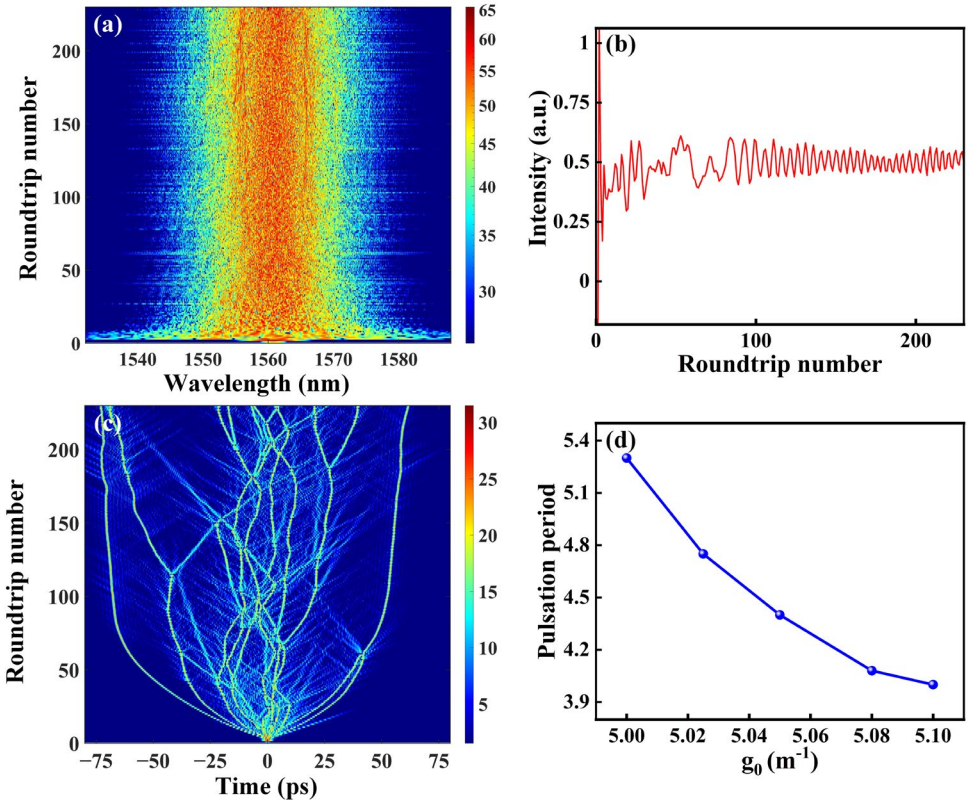

Figure 9. Simulating pulsating NLPs. (**a**) Evolutions of the spectra. (**b**) Energy evolutions. (**c**) Pulse evolutions. (**d**) Pulsation periods with different small signal gain values.

Numerical simulations reveal that, under appropriate settings of other parameters, the generation of NLPs and pulsating characteristics are primarily induced by an increase in the small-signal gain. This indicates that pulsating NLPs arise from the combined effects of intracavity gain saturation and nonlinear interactions, which manifest through variations in pump power and polarization state. Specifically, the enhancement of gain, constrained by the peak-power clamping effect, drives soliton pulses toward splitting [35]. This process causes the collapse of stable mode-locking and the establishment of an NLP regime with chaotic properties. On this basis, strong and weak interactions among chaotic solitons may represent a crucial factor contributing to the onset of pulsation behavior [36,37]. Therefore,

with a proper cavity design, considering the balance among various factors (such as gain, loss, dispersion, and nonlinearity), the generation of pulsating NLPs can be achieved in experiments.

5. Conclusions

In conclusion, we have investigated the generation and evolution of pulsating NLPs in an ultrafast fiber laser. By properly increasing the pump power and adjusting the polarization state, the laser can be driven from the stable mode-locked state into the pulsating NLP regime. The real-time spectral measurements reveal that both the spectrum and pulse energy of the pulsating NLPs vary periodically, which is a distinctive characteristic of pulsating solitons. Within a single period, the spectral intensity and wave-packet profile display irregular fluctuations, reflecting the chaotic property of the NLP state. Furthermore, numerical simulations are performed to analyze the dynamics of the pulsating NLPs, offering additional theoretical support for the experimental observations. It is reasonable to conclude that our findings enrich the study of soliton dynamics and pave the way for further investigations into nonlinear pulse behaviors.

Author Contributions: Conceptualization, Z.W.; methodology, Z.W.; software, P.T.; validation, L.Z.; formal analysis, L.Z. and J.Z.; investigation, Z.Z.; resources, Z.W.; data curation, H.W.; writing—original draft preparation, L.Z., J.Z. and Z.Z.; visualization, L.Z.; writing—review and editing, Z.W.; supervision, Z.W.; project administration, Z.W.; funding acquisition, Z.W. All authors have read and agreed to the published version of the manuscript.

Funding: This work was supported by the Hunan Provincial Natural Science Foundation of China (Grant No. 2023JJ30596), the Guangdong Basic and Applied Basic Research Foundation (Grant Nos. 2023A1515010093, 2024A1515012152, and 2025A1515012351), and the Shenzhen Fundamental Research Program (Grant Nos. JCYJ20231121110828001, JCYJ20231121113641002, and JCYJ20230808105713028).

Data Availability Statement: Data underlying the results presented in this paper are not publicly available at this time but may be obtained from the authors upon reasonable request.

Conflicts of Interest: The authors declare no conflicts of interest.

References

1. Chang, G.; Wei, Z. Ultrafast Fiber Lasers: An Expanding Versatile Toolbox. *iScience* **2020**, *23*, 101101. [CrossRef]
2. Fermann, M.E.; Hartl, I. Ultrafast Fibre Lasers. *Nat. Photonics* **2013**, *7*, 868–874. [CrossRef]
3. Ma, J.; Qin, Z.; Xie, G.; Qian, L.; Tang, D. Review of Mid-Infrared Mode-Locked Laser Sources in the 2.0 μm–3.5 μm Spectral Region. *Appl. Phys. Rev.* **2019**, *6*, 021317. [CrossRef]
4. Fermann, M.E.; Hartl, I. Ultrafast Fiber Laser Technology. *IEEE J. Sel. Top. Quantum Electron.* **2009**, *15*, 191–206. [CrossRef]
5. Song, Y.; Shi, X.; Wu, C.; Tang, D.; Zhang, H. Recent Progress of Study on Optical Solitons in Fiber Lasers. *Appl. Phys. Rev.* **2019**, *6*, 021313. [CrossRef]
6. Grelu, P.; Akhmediev, N. Dissipative Solitons for Mode-Locked Lasers. *Nat. Photonics* **2012**, *6*, 84–92. [CrossRef]
7. Mao, D.; Liu, X.; Han, D.; Lu, H. Compact All-Fiber Laser Delivering Conventional and Dissipative Solitons. *Opt. Lett.* **2013**, *38*, 3190–3193. [CrossRef]
8. Liu, M.; Luo, A.-P.; Xu, W.-C.; Luo, Z.-C. Dissipative Rogue Waves Induced by Soliton Explosions in an Ultrafast Fiber Laser. *Opt. Lett.* **2016**, *41*, 3912–3915. [CrossRef]
9. Luo, Z.-C.; Liu, M.; Liu, H.; Zheng, X.-W.; Luo, A.-P.; Zhao, C.-J.; Zhang, H.; Wen, S.-C.; Xu, W.-C. 2 GHz Passively Harmonic Mode-Locked Fiber Laser by a Microfiber-Based Topological Insulator Saturable Absorber. *Opt. Lett.* **2013**, *38*, 5212–5215. [CrossRef]
10. Bale, B.G.; Kieu, K.; Kutz, J.N.; Wise, F. Transition Dynamics for Multi-Pulsing in Mode-Locked Lasers. *Opt. Express* **2009**, *17*, 23137–23146. [CrossRef]
11. Kbashi, H.J.; Sergeyev, S.V.; Araimi, M.A.; Tarasov, N.; Rozhin, A. Vector Soliton Rain. *Laser Phys. Lett.* **2019**, *16*, 035103. [CrossRef]
12. Turnali, A.; Xu, S.; Sander, M.Y. Noise-like Pulse Generation and Amplification from Soliton Pulses. *Opt. Express* **2022**, *30*, 13977–13984. [CrossRef]

13. Chen, H.-J.; Tan, Y.-J.; Long, J.-G.; Chen, W.-C.; Hong, W.-Y.; Cui, H.; Luo, A.-P.; Luo, Z.-C.; Xu, W.-C. Dynamical Diversity of Pulsating Solitons in a Fiber Laser. *Opt. Express* **2019**, *27*, 28507–28522. [CrossRef]
14. Wei, Z.-W.; Liu, M.; Ming, S.-X.; Cui, H.; Luo, A.-P.; Xu, W.-C.; Luo, Z.-C. Exploding Soliton in an Anomalous-Dispersion Fiber Laser. *Opt. Lett.* **2020**, *45*, 531–534. [CrossRef]
15. Runge, A.F.J.; Broderick, N.G.R.; Erkintalo, M. Observation of Soliton Explosions in a Passively Mode-Locked Fiber Laser. *Optica* **2015**, *2*, 36–39. [CrossRef]
16. Wei, Z.-W.; Liu, M.; Ming, S.-X.; Luo, A.-P.; Xu, W.-C.; Luo, Z.-C. Pulsating Soliton with Chaotic Behavior in a Fiber Laser. *Opt. Lett.* **2018**, *43*, 5965–5968. [CrossRef]
17. Peng, J.; Boscolo, S.; Zhao, Z.; Zeng, H. Breathing Dissipative Solitons in Mode-Locked Fiber Lasers. *Sci. Adv.* **2019**, *5*, eaax1110. [CrossRef]
18. He, R.; Wang, Z.; Liu, Y.; Wang, Z.; Liang, H.; Han, S.; He, J. Dynamic Evolution of Pulsating Solitons in a Dissipative System with the Gain Saturation Effect. *Opt. Express* **2018**, *26*, 33116–33128. [CrossRef]
19. Chang, W.; Soto-Crespo, J.M.; Vouzas, P.; Akhmediev, N. Extreme Soliton Pulsations in Dissipative Systems. *Phys. Rev. E* **2015**, *92*, 022926. [CrossRef]
20. Wang, X.; Liu, Y.; Wang, Z.; Yue, Y.; He, J.; Mao, B.; He, R.; Hu, J. Transient Behaviors of Pure Soliton Pulsations and Soliton Explosion in an L-Band Normal-Dispersion Mode-Locked Fiber Laser. *Opt. Express* **2019**, *27*, 17729–17742. [CrossRef]
21. Chen, J.; Zhao, X.; Li, T.; Yang, J.; Liu, J.; Zheng, Z. Generation and Observation of Ultrafast Spectro-Temporal Dynamics of Different Pulsating Solitons from a Fiber Laser. *Opt. Express* **2020**, *28*, 14127–14133. [CrossRef]
22. Ji, Y.; Yang, Y.; Song, Y.; Wang, K.; Du, G.; Liu, J.; Tang, D.; Wang, Z. Dynamics of Pulsating Solitons with Chaotic Behaviors from a 1.7 μm Ultrafast Fiber Laser. *Chaos Solitons Fractals* **2024**, *187*, 115379. [CrossRef]
23. Soto-Crespo, J.M.; Grelu, P.; Akhmediev, N.; Devine, N. Soliton Complexes in Dissipative Systems: Vibrating, Shaking, and Mixed Soliton Pairs. *Phys. Rev. E* **2007**, *75*, 016613. [CrossRef] [PubMed]
24. Chang, W.; Ankiewicz, A.; Akhmediev, N.; Soto-Crespo, J.M. Creeping Solitons in Dissipative Systems and Their Bifurcations. *Phys. Rev. E* **2007**, *76*, 016607. [CrossRef] [PubMed]
25. Akhmediev, N.; Soto-Crespo, J.M.; Town, G. Pulsating Solitons, Chaotic Solitons, Period Doubling, and Pulse Coexistence in Mode-Locked Lasers: Complex Ginzburg-Landau Equation Approach. *Phys. Rev. E* **2001**, *63*, 056602. [CrossRef]
26. Chen, T.-H.; Lin, Y.-H.; Cheng, C.-H.; Tsai, C.-T.; Chi, Y.-C.; Lin, G.-R. Unintentional Polarization Dependent Pulsewidth of Graphene Mode-Locked Er-Doped Fiber Lasers. *IEEE J. Sel. Top. Quantum Electron.* **2017**, *23*, 50–59. [CrossRef]
27. Runge, A.F.J.; Hudson, D.D.; Tam, K.K.K.; de Sterke, C.M.; Blanco-Redondo, A. The Pure-Quartic Soliton Laser. *Nat. Photonics* **2020**, *14*, 492–497. [CrossRef]
28. Runge, A.F.J.; Aguergaray, C.; Broderick, N.G.R.; Erkintalo, M. Coherence and Shot-to-Shot Spectral Fluctuations in Noise-like Ultrafast Fiber Lasers. *Opt. Lett.* **2013**, *38*, 4327–4330. [CrossRef]
29. Man, W.S.; Tam, H.Y.; Demokan, M.S.; Wai, P.K.A.; Tang, D.Y. Mechanism of Intrinsic Wavelength Tuning and Sideband Asymmetry in a Passively Mode-Locked Soliton Fiber Ring Laser. *J. Opt. Soc. Am. B* **2000**, *17*, 28–33. [CrossRef]
30. Jeong, Y.; Vazquez-Zuniga, L.A.; Lee, S.; Kwon, Y. On the Formation of Noise-like Pulses in Fiber Ring Cavity Configurations. *Opt. Fiber Technol.* **2014**, *20*, 575–592. [CrossRef]
31. Luo, A.-P.; Luo, Z.-C.; Liu, H.; Zheng, X.-W.; Ning, Q.-Y.; Zhao, N.; Chen, W.-C.; Xu, W.-C. Noise-like Pulse Trapping in a Figure-Eight Fiber Laser. *Opt. Express* **2015**, *23*, 10421–10427. [CrossRef] [PubMed]
32. Zhou, Y.; Yang, K.; Tsia, K.K.; Zeng, H.; Wong, K.K.Y. Intelligent Soliton Molecules Control in an Ultrafast Thulium Fiber Laser. *Adv. Photonics Nexus* **2025**, *4*, 016012. [CrossRef]
33. Wang, X.; Li, K.; Lu, M.; Fan, Y.; Fu, M.; Xu, A.; Li, S. Pulsating Dynamics of Noise-like Pulses in a Fiber Laser with Nonlinear Optical Loop Mirror. *Laser Phys. Lett.* **2024**, *21*, 085102. [CrossRef]
34. Han, Y.; Gao, B.; Wu, G.; Huo, J.-Y.; Wen, H.-L.; Li, Y.-Y.; Liu, L.; Ma, C.-Y. Creeping and Erupting Dynamics in a Pure-Quartic Soliton Fiber Laser. *Opt. Express* **2023**, *31*, 1787–1798. [CrossRef]
35. Tang, D.Y.; Zhao, L.M.; Zhao, B.; Liu, A.Q. Mechanism of Multisoliton Formation and Soliton Energy Quantization in Passively Mode-Locked Fiber Lasers. *Phys. Rev. A* **2005**, *72*, 043816. [CrossRef]
36. Liu, J.; Li, M.; He, J.; Song, Y.; Wang, Z. Noisy Soliton Pulsation and Its Dynamics in a Mid-Infrared Ultrafast Fiber Laser. *Chaos Solitons Fractals* **2023**, *177*, 114199. [CrossRef]
37. Wang, Z.; Wang, X.; Song, Y.; Liu, J.; Zhang, H. Generation and Pulsating Behaviors of Loosely Bound Solitons in a Passively Mode-Locked Fiber Laser. *Phys. Rev. A* **2020**, *101*, 013825. [CrossRef]